

A nicotinamide metabolism-related gene signature for predicting immunotherapy response and prognosis in lung adenocarcinoma patients

Meng Wang^{1,2}, Wei Li^{1,2}, Fang Zhou^{1,2}, Zheng Wang^{1,2}, Xiaoteng Jia³ and Xingpeng Han^{1,2}

¹ Department of Thoracic Surgery, Tianjin Chest Hospital, Tianjin, China

² Chest Hospital, Tianjin University, Tianjin, China

³ Clinical School of Thoracic, Tianjin Medical University, Tianjin, China

ABSTRACT

Background: Nicotinamide (NAM) metabolism fulfills crucial functions in tumor progression. The present study aims to establish a NAM metabolism-correlated gene (NMRG) signature to assess the immunotherapy response and prognosis of lung adenocarcinoma (LUAD).

Methods: The training set and validation set (the GSE31210 dataset) were collected from The Cancer Genome Atlas (TCGA) and Gene Expression Omnibus (GEO), respectively. Molecular subtypes of LUAD were classified by consensus clustering. Mutation landscape of the top 20 somatic genes was visualized by maftools package. Subsequently, differential expression analysis was conducted using the limma package, and univariate, multivariate and LASSO regression analyses were performed on the screened genes to construct a risk model for LUAD. Next, the MCP-counter, TIMER and ESTIMATE algorithms were utilized to comprehensively assess the immune microenvironmental profile of LUAD patients in different risk groups. The efficacy of immunotherapy and chemotherapy drugs was evaluated by TIDE score and pRRophetic package. A nomogram was created by integrating RiskScore and clinical features. The mRNA expressions of independent prognostic NMRGs and the migration and invasion of LUAD cells were measured by carrying out cellular assays.

Results: Two subtypes (C1 and C2) of LUAD were classified, with C1 subtype showing a worse prognosis than C2. The top three genes with a high mutation frequency in C1 and C2 subtypes were *TTN* (45.25%), *FLG* (25.25%), and *ZNF536* (19.8%). Four independent prognostic NMRGs (*GJB3*, *CPA3*, *DKK1*, *KRT6A*) were screened and used to construct a RiskScore model, which exhibited a strong predictive performance. High-risk group showed low immune cell infiltration, high TIDE score, and worse prognosis, and the patients in this group exhibited a high drug sensitivity to Cisplatin, Erlotinib, Paclitaxel, Saracatinib, and CGP_082996. A nomogram was established with an accurate predictive and diagnostic performance. *GJB3*, *DKK1*, *CPA3*, and *KRT6A* were all high-expressed in LUAD cells, and silencing *GJB3* inhibited the migration and invasion of LUAD cells.

Conclusion: A novel NMRG signature was developed, contributing to the prognostic evaluation and personalized treatment for LUAD patients.

Submitted 7 November 2024

Accepted 23 January 2025

Published 27 February 2025

Corresponding author

Xingpeng Han,
hxingpeng19652023@163.com

Academic editor

Huashan Shi

Additional Information and
Declarations can be found on
page 21

DOI 10.7717/peerj.18991

© Copyright
2025 Wang et al.

Distributed under
Creative Commons CC-BY 4.0

OPEN ACCESS

Subjects Biochemistry, Bioinformatics, Cell Biology, Immunology, Oncology

Keywords Nicotinamide metabolism, Tumor microenvironment, Lung adenocarcinoma, Metabolic reprogramming, Prognosis, immunotherapy

INTRODUCTION

Lung cancer is a frequent and lethal epithelial malignant tumor (*Tang et al., 2023; Zhang et al., 2023*). In 2020, China reported approximately 820,000 new cases of lung cancer, constituting 17.9% of all new cancer diagnoses (4.57 million), with 710,000 fatalities, which accounted for 23.7% of all cancer-related deaths (3 million) (*Cao et al., 2023*). Lung adenocarcinoma (LUAD), the predominant subtype of lung cancer, comprises more than 40% of all lung cancer cases and is characterized by its aggressive nature and high mortality rate (*Cao et al., 2024; Xia et al., 2024*). Despite advancements including chemotherapy, surgical resection, radiotherapy, immunotherapy, and targeted molecular therapies, the prognosis of lung cancer remains grim (*Meng et al., 2024; Zhou et al., 2022; Ding, Lv & Hua, 2022*). This is largely due to the challenges in early detection, rapid progression of the cancer as well as the development of treatment resistance (*Zhang et al., 2022; Zheng et al., 2023*). Immunotherapy is a promising strategy for treating LUAD, and studies have shown the crucial role of immune system in LUAD progression (*Guo et al., 2022*). Specifically, immune checkpoint inhibitors (ICIs) have become a pivotal therapeutic modality LUAD for and are widely applied in clinical setting (*Xu et al., 2023*). In China, the currently approved ICIs for LUAD treatment are mainly PD-1 and PD-L1 inhibitors, including agents such as tislelizumab, pembrolizumab, and durvalumab (*Feng et al., 2023; Hu et al., 2022*). However, due to tumor heterogeneity of tumors and patient-specific differences, only about 15% of patients could benefit from ICIs (*Nguyen et al., 2022; He et al., 2024*). Studies confirmed that developing risk models and analyzing immune infiltration analysis in both low- and high-risk groups can assist in predicting the immune therapeutic response in LUAD (*Li et al., 2023; Yi et al., 2021; Wu et al., 2021*). Hence, establishing risk model for LUAD prognosis is imperative, as they can inform treatment strategies and improve patient outcomes.

Metabolic reprogramming is a hallmark of malignant tumors, primarily involving alterations in glutamine metabolism, glucose metabolism, and lipid metabolism (*Li et al., 2022; Zhang, Zou & Fang, 2023*). This reprogramming allows tumors to evade cell apoptosis, a prerequisite for promoting rapid proliferation, invasion, and metastasis of tumor cells (*Shum et al., 2023*). It has been reported that metabolic reprogramming not only enables cancer cells to escape immune surveillance, but also induces treatment resistance and interacts with the tumor microenvironment *via* the metabolites produced (*Faubert, Solmonson & DeBerardinis, 2020*). Inhibition of metabolic reprogramming could reduce tumor aggressiveness (*Liu et al., 2023*), thus identifying it as a possible target for cancer therapies (*Nong et al., 2023*). Nicotinamide (NAM), the amide pattern of vitamin B3, serves as a precursor to nicotinamide-adenine dinucleotide (NAD⁺), a key mediator in cellular energy metabolism (*Song et al., 2019*). During cell senescence, the reduction of NAD⁺ levels will increase the production of reactive oxygen species (ROS), contributing to

metabolic reprogramming (Cui et al., 2023). Increasing evidence demonstrated the pivotal role of NAM in the prevention and therapies of cancers (Nikas, Paschou & Ryu, 2020). For example, NAM could suppress breast cancer cell proliferation *via* mitochondrial dysfunction and ROS accumulation by regulating lipid metabolism pathway (Jung et al., 2022). As a crucial enzyme in the NAD⁺ salvage pathway, nicotinamide phosphoribosyl transferase (NAMPT) could convert NAM to nicotinamide mononucleotide (NMN), contributing significantly to immunosuppressive microenvironment (Burgos, 2011; Travelli et al., 2019). In certain tumors, NAMPT has been found to promote the expression of PD-L1, which allows tumors to evade immune response, particularly in a CD8⁺ T cell-dependent manner (Li et al., 2020; Lv et al., 2021). These findings highlighted the significance and potential prognostic value of NAM metabolism in relation to tumor outcomes and immune responses.

Given that the research on the correlation between NAM metabolism and immunotherapy response and prognosis of LUAD is limited, the present research set out to examine the significant role of NAM metabolism in LUAD progression and to develop a new predictive model for immunotherapeutic response and prognosis based on NAM metabolism-related genes (NMRGs). Firstly, molecular subtypes of LUAD were delineated using NMRGs, and comparisons were made regarding clinical features, somatic gene mutation profiles, and differentially expressed genes (DEGs) across the subtypes. Subsequently, independent prognostic NMRGs were screened to create a RiskScore model for patients suffering from LUAD, the reliability of which was validated using GSE31210 dataset. The analysis extended to assessing immune infiltration, immunotherapy response, and drugs sensitivity across different risk groups. Furthermore, a nomogram integrating RiskScore with clinical features was established. Finally, the mRNA expressions of independent prognostic NMRGs, and cell migration and invasion capabilities of LUAD cells were experimentally verified. This study offers a promising method for evaluating the prognostic outcomes and treatment effectiveness for LUAD patients, potentially improving clinical decision-making.

MATERIALS AND METHODS

Data collection and preprocessing

The somatic mutation information and clinical phenotype data of LUAD were collected from the Cancer Genome Atlas (TCGA) database (<https://portal.gdc.cancer.gov/>). The RNA-seq expression profile was converted to FPKM format and log₂-converted. The somatic gene mutation information was processed by mutect2 (Saba et al., 2020). After removing samples that lacked survival time or survival status, a total of 500 tumor samples with a survival time longer than 0 day were obtained.

The chip data of GSE31210 (Shahrajabian & Sun, 2023) was acquired from Gene Expression Omnibus (GEO) (<https://www.ncbi.nlm.nih.gov/geo/query/acc.cgi?acc=GSE31210>) (Song et al., 2023). The probes were transformed to genes symbol based on the annotation information. A total of 226 tumor samples from GSE31210 were recruited

for subsequent study after removing normal samples and those without clinical follow-up or overall survival (OS) data.

TCGA-LUAD and GSE31210 datasets served as the training dataset and independent validation dataset, respectively.

Consensus clustering analysis

Firstly, 42 NMRGs obtained from a previous study (Cui *et al.*, 2023) were subjected to univariate Cox regression analysis ($p < 0.05$) to filter prognostically significant NMRGs in LUAD. Then, consensus clustering was performed to delineate molecular subtypes of TCGA-LUAD using ConsensusClusterPlus R package (the parameters were set as clusterAlg = “hc” and distance = “Spearman”) (Li *et al.*, 2020). Sampling was repeated 500 times with 80% samples involved each time. The optimal cluster number (between 2 to 10) was determined according to the CDF. Finally, the prognosis between different subtypes in TCGA-LUAD cohort was evaluated and validated in GSE31210 dataset.

Somatic gene mutation landscape analysis

Somatic genes with mutation frequencies higher than 2 were selected. Then, genes with significantly high mutation frequencies within each molecular subtype were further identified using Fisher’s exact test, setting a threshold of $p < 0.05$. Next, the mutation landscape of the top 20 somatic genes in each molecular subtype was visually displayed using a waterfall diagram, generated with the maftools R package (Jia *et al.*, 2024).

Identification of DEGs and GSEA

DEGs among different subtypes of TCGA-LUAD were selected using limma R package, with a screening threshold of $|\log_2\text{FoldChange (FC)}| > \log_2(1.5)$ and $p < 0.05$. Following this, pathway enrichment analysis was conducted *via* GSEA R package to pinpoint significantly enriched pathways, using a threshold of $p < 0.05$ (Innis *et al.*, 2021). The gene set “h.all.v2023.1.Hs.entrez.gmt” from the MsigDB (<https://www.gsea-msigdb.org/gsea/msigdb/>) served as the background gene sets (Li *et al.*, 2023), encompassing the HALLMARK series of pathways.

Development and verification of a RiskScore model

Using univariate Cox regression analysis ($p < 0.05$), the prognostic genes were selected from the DEGs between the molecular subtypes in TCGA-LUAD. Subsequently, the model was refined by performing LASSO Cox regression analysis in the glmnet R package and 10-fold cross validation (Li *et al.*, 2024). Then, the independent prognostic NMRGs were screened *via* stepwise multivariate regression analysis and applied to develop the RiskScore model as follow (Fan *et al.*, 2024):

$$\text{RiskScore} = \sum \beta_i * \text{Exp}_i$$

β_i indicates the coefficient of gene in Cox regression model, and Exp_i represents gene expression value.

The RiskScore for all the samples in TCGA-LUAD and GSE31210 datasets was calculated, and LUAD patients were separated by the median RiskScore value into high- and low-risk groups. The ROC curve was constructed using timeROC R package (Zhang, 2022). The model robustness was validated using the GSE31210 dataset.

Evaluation of the TME

To investigate the association between the TME in LUAD and different risk groups, the scores of a total of 28 types of tumor infiltration immune cells (TIICs) were computed for each sample (Wang et al., 2020). Also, the scores of 10 types of immune cells were calculated by MCP-counter (Zhang et al., 2022). The TIMER online tool (<http://cistrome.org/TIMER>) was employed to calculate the scores of six immune cells (Cao et al., 2022). Moreover, ESTIMATE algorithm was utilized to output the ESTIMATEScore, StromalScore, ImmuneScore using estimated R package (Ke et al., 2021).

Immunotherapy response and drug sensitivity assessment

Firstly, the TIDE score was calculated based on the standardized transcriptome data in TIDE website (<http://tide.dfci.harvard.edu/>) (Zheng et al., 2024) to evaluate the immunotherapy response of LUAD patients, with higher TIDE scores indicating greater immune escape possibility and less immunotherapy benefit. Furthermore, the sensitivity of LUAD patients in TCGA-LUAD to 10 common chemotherapy drugs was compared based on the IC₅₀ value using pRRopetic R package.

Development and verification of a NAM metabolism-related nomogram

Firstly, independent prognostic factors were identified by subjecting clinical traits and RiskScore model to univariate and multivariate Cox regression analysis. Then, a nomogram integrating RiskScore with other clinicopathologic features was created to evaluate the 1-, 3-, and 5- year survival rate of patients with LUAD (Liu et al., 2024). The nomogram's performance was assessed using a calibration curve and DCA. The predictive accuracy was further validated by calculating the C-index (Wang et al., 2022). Additionally, the diagnostic efficacy of the nomogram was evaluated through plotting receiver operating characteristic (ROC) curves using the timeROC R package (Lin et al., 2023).

Cell culture and transfection

Normal human lung epithelial cell line (BEAS-2B) and the LUAD cell line (A549) were procured from Wuhan Sunncell Biotechnology Co., Ltd (Wuhan, China). DMEM/F12 medium comprising 10% fetal bovine serum (FBS) and 1% penicillin-streptomycin was used in all cell culture under the incubation conditions of 37 °C, 5% CO₂, and saturated humidity.

Subsequently, the silencing of *GJB3* was conducted by cell transfection. The small interfering (si) RNA specifically targeting *GJB3* (si-*GJB3*) along with a negative control (si-NC) was obtained (Shanghai Sangon Biotechnology Co., Ltd., Shanghai, China). The sequence of si-*GJB3* was AAGTTATGCAACTTTCGTTTTGG. Transfection of A549 cells

was conducted with the use of Lipofectamine® 3000 (Invitrogen, Thermo Fisher Scientific) for 48 h, according to the instruction.

Quantitative real-time PCR

Firstly, the total RNA of BEAS-2B and A549 cells obtained using TriZol reagent (Invitrogen, Waltham, MA, USA) was reverse-transcribed into cDNA with SuperScript IV reverse transcriptase (Invitrogen, Waltham, MA, USA). Next, to measure the mRNA expressions of independent prognostic NMRGs in BEAS-2B and A549 cells, quantitative real-time PCR (qRT-PCR) was conducted for amplification using SYBR® Premix Ex Taq™ II (Takara, Shanghai, China). See [Table S1](#) for the primer sequences. The amplification was performed as follows: pre-denaturation at 95 °C for 1 minute (min), 40 cycles of 95 °C for 30 seconds (s), and annealing at 56 °C for 30 s, elongation at 72 °C for 40 s. The relative expressions of NMRGs were quantified by $2^{-\Delta\Delta CT}$ method, applying *GAPDH* as the housekeeping gene ([Song et al., 2023](#)).

Wound-healing assay

The A549 cell migration was measured by wound-healing assay ([Zhang et al., 2022](#)). A549 cells at a concentration of 2×10^5 cells/well were cultured in a 24-well plate and scratched using an aseptic pipette tip. After washing with phosphate buffer, the A549 cells were cultivated in serum-free medium. The BX53M upright metallographic microscope (Olympus, Tokyo, Japan) was applied to observe and capture the representative images at 0 and 48 h. Meanwhile, the wound closure (%) of A549 cells was counted.

Transwell assay

Transwell assay was conducted to evaluate the invasion of A549 cells ([Zhou et al., 2021](#)). Firstly, each Transwell chamber was added with 70 μ L diluted Matrigel and placed at 37 °C for 2 h to coagulate the Matrigel. Then, the A549 cells (2×10^5 cells/well) were suspended in 250 μ L non-serum medium contained in the upper chamber and incubated, while 650 μ L medium comprising 10% FBS was supplemented to the lower chamber. Following 24-h cultivation, 5% paraformaldehyde was used to fix the A549 cells invading the lower chamber for 30 min. Then, 0.1% crystal violet was employed to dye the fixed cells for 15 min. Finally, the invaded A549 cells were quantified under the BX53M upright metallic microscope (Olympus, Tokyo, Japan).

Statistical analysis

Bioinformatic analysis were performed using R software 4.2.1. Two-group differences were calculated by Wilcoxon rank test. The distribution of clinicopathologic features was analyzed by Chi-Squared test. Survival differences among different risk groups or subtypes were compared by Kaplan-Meier curves. Data were shown as mean \pm standard deviation, and GraphPad Prism 7.0 was employed to conduct statistical analysis. Student's *t*-test was employed to test two-group comparisons. And $p < 0.05$ was considered statistically significant.

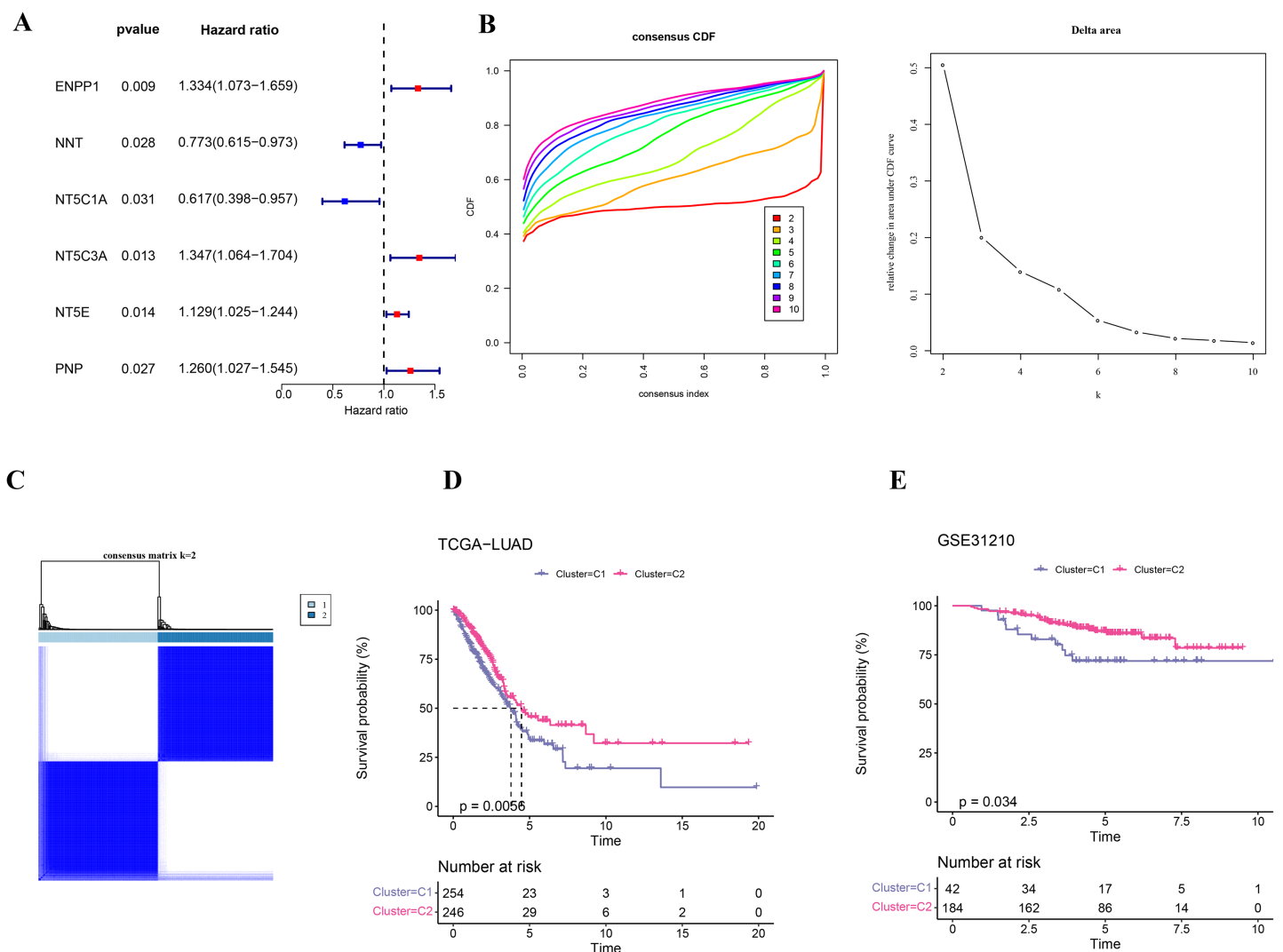


Figure 1 Identification on the molecular subtypes of LUAD based on NMRGs. (A) The NMRGs associated with prognosis. (B) Consensus cumulative distribution function (CDF) and CDF Delta area curves in TCGA-LUAD cohort. (C) Heatmap of consensus matrix in TCGA-LUAD cohort. (D) Overall survival (OS) difference between two molecular subtypes in TCGA-LUAD cohort. (E) OS curve of two molecular subtypes in GSE31210. Full-size [DOI: 10.7717/peerj.18991/fig-1](https://doi.org/10.7717/peerj.18991/fig-1)

RESULTS

Using NMRGs to classify two molecular subtypes of LUAD

Firstly, six NMRGs (*ENPP1*, *NNT*, *NT5C1A*, *NT5C3A*, *NT5E*, and *PNP*) were significantly correlated with the prognostic outcomes of LUAD (Fig. 1A). Using these six NMRGs, consensus clustering analysis was performed on the 500 samples in TCGA-LUAD dataset. According to the CDF and CDF Delta area curves, the clustering results were stable when there were two clusters (Fig. 1B). Thus, LUAD patients were divided into two subtypes when consensus matrix $k = 2$ (Fig. 1C). In TCGA-LUAD cohort, the OS probability in C2 subtype was more favorable than that in C1 subtype (Fig. 1D), indicating that C2 subtype patients exhibited a better prognosis than C1 subtype. In addition, 226 samples in

GSE31210 dataset were similarly clustered into two stable subtypes, which also showed clear prognostic differences (Fig. 1E).

Clinical features and somatic gene mutation landscape between the two subtypes

Comparison on the distribution difference of clinicopathologic features between C1 and C2 in TCGA-LUAD cohort showed that compared to C2 subtype, more patients in C1 subtype were in the pathologic_M1, pathologic_T3, T4, pathologic_N1, N2, and pathologic_stage II, III (Figs. 2A–2D). In addition, 369 somatic mutation genes with significantly high mutation frequency between C1 and C2 subtypes were obtained and the mutation distribution of the top 20 genes was visually displayed. The top three somatic genes with the highest mutation frequencies were *TTN* (45.25%), *FLG* (25.25%), and *ZNF536* (19.8%) (Fig. 2E).

DEGs were identified and GSEA was performed between two subtypes

Firstly, DEG analysis between C1 and C2 in TCGA-LUAD cohort screened 178 upregulated DEGs and 61 downregulated DEGs (Fig. 3A). Furthermore, GSEA showed that C1 subtype was specifically enriched in multiple pathways, including the P53_PATHWAY, GLYCOLYSIS, TGF_BETA_SIGNALING, KRAS_SIGNALING_UP, HYPOXIA, which are associated with the progression and deterioration of tumors (Fig. 3B). However, C2 subtype was enriched in the pathways such as MTORC1_SIGNALING, FATTY_ACID_METABOLISM, MYC_TARGETS_V2, and REACTIVE_OXYGEN_SPECIES_PATHWAY (Fig. 3B). These results showed that C1 subtype was more associated with glycolytic metabolism-related pathways, while C2 subtype was more related to fatty acid metabolism pathway.

RiskScore model with a high prediction performance was constructed

Univariate Cox regression analysis screened 88 genes significantly related to LUAD prognosis between C1 and C2 ($p < 0.05$). To refine the risk model, LASSO Cox regression analysis with 10-fold cross validation was performed to reduce gene number (Figs. 4A and 4B). Subsequently, four independent prognostic NMRGs, including 1 protective gene (*CPA3*) and three risk genes (*DKK1*, *GJB3*, *KRT6A*), were screened by multivariate Cox regression analysis (Fig. 4C) and used to establish a RiskScore model:

$$\text{RiskScore} = (0.095 * GJB3) + (-0.141 * CPA3) + (0.155 * DKK1) + (0.046 * KRT6A).$$

A total of 500 samples in TCGA-LUAD were divided by the median RiskScore value into low-risk and high-risk groups (Fig. 4D). Furthermore, the AUC displayed that the RiskScore model was credible with 1-, 3-, and 5- year AUC of 0.74, 0.68, and 0.62, respectively (Fig. 4E). In TCGA-LUAD cohort, Kaplan-Meier curves demonstrated that low-risk group had better survivals in terms of progression-free interval (PFI), OS, disease-specific survival (DSS), and disease-free interval (DFI) (Figs. 4F–4I), which suggested that patients with a high RiskScore had a worse prognosis.

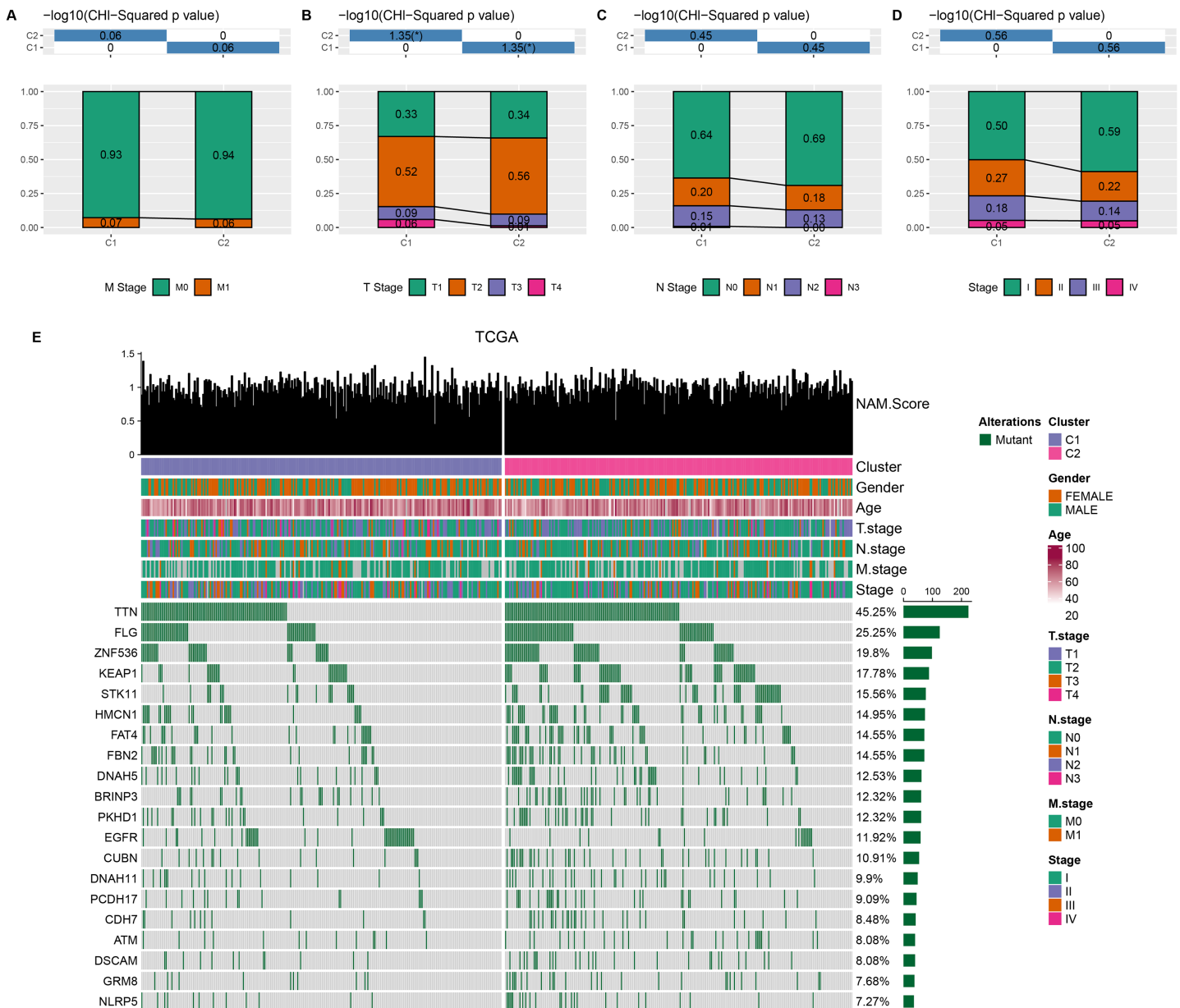


Figure 2 Clinical features and somatic gene mutation landscape between two molecular subtypes. (A–D) The distribution difference of clinical features between two molecular subtypes in TCGA-LUAD cohort, including M Stage, T Stage, N Stage, and Stage. * means $p < 0.05$. (E) The somatic gene mutation landscape between two molecular subtypes in TCGA-LUAD cohort. [Full-size DOI: 10.7717/peerj.18991/fig-2](https://doi.org/10.7717/peerj.18991/fig-2)

The RiskScore model was validated in GSE31210 dataset

To confirm the stability and reliability of RiskScore model, the GSE31210 dataset containing 226 tumor samples served as an independent validation set. Similarly, the results in validation cohort were in line with those in TCGA-LUAD training set. In detail, 226 tumor samples in GSE31210 dataset were divided into low- and high-risk groups (Fig. 5A), with low-risk patients having a higher OS probability (Fig. 5C). This suggested that the prognostic outcomes of low-risk patients were more favorable than the high-risk patients. The ROC curve also validated the reliability of the RiskScore model, with 1-, 3-,

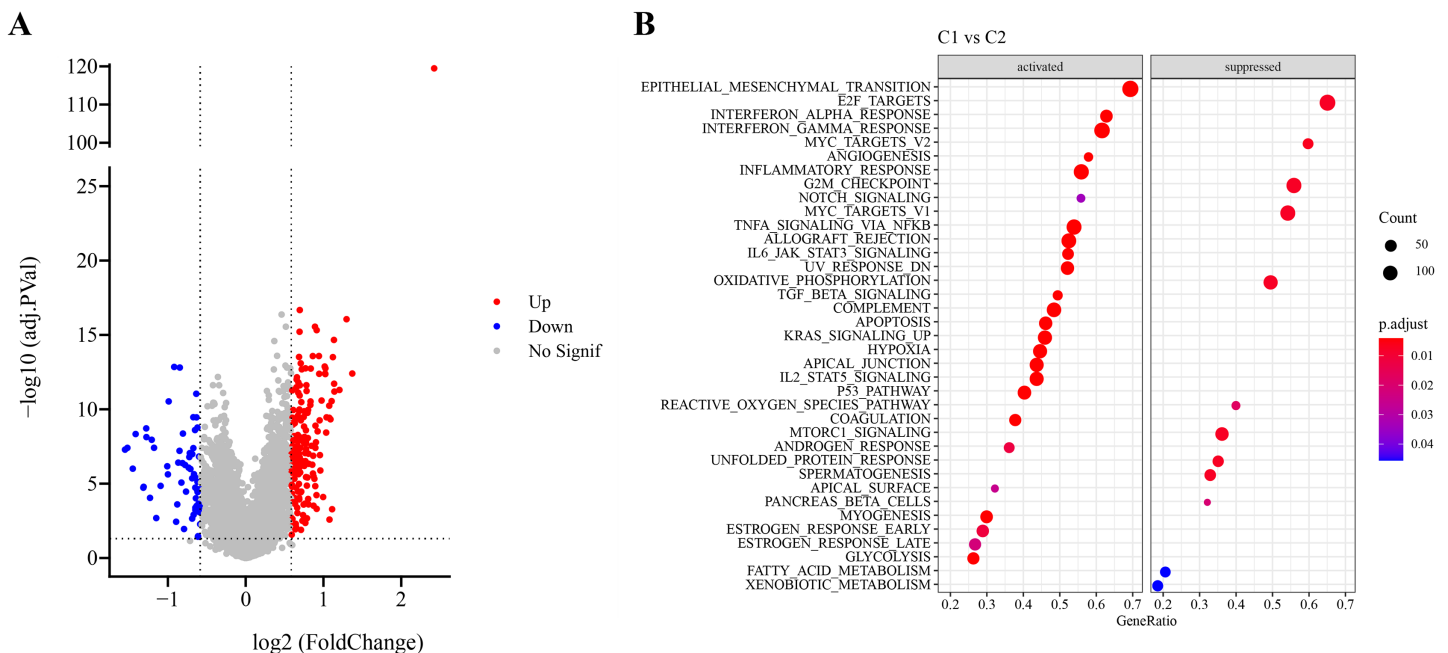


Figure 3 Identification and pathway enrichment analysis of differentially expressed genes (DEGs). (A) Volcano map of DEGs between two molecular subtypes in TCGA-LUAD cohort. (B) HALLMARK pathway enrichment results of DEGs between two molecular subtypes.

Full-size [DOI: 10.7717/peerj.18991/fig-3](https://doi.org/10.7717/peerj.18991/fig-3)

and 5-year AUC of 0.74, 0.69, and 0.59, respectively (Fig. 5B). Moreover, to further investigate the roles of the four model genes (*GJB3*, *CPA3*, *DKK1*, *KRT6A*) in LUAD prognosis, 226 patients in GSE31210 dataset were divided by the median expression of these genes into high- and low- expression groups. Except for *DKK1*, the expressions of *GJB3*, *CPA3*, and *KRT6A* were closely linked to the OS of LUAD patients. The low expression groups of *GJB3* and *KRT6A* exhibited better OS than high expression groups, while the high expression group of *CPA3* had higher OS rate than low expression group (Fig. 5D), indicating that the expressions of these model genes could affect LUAD prognosis.

Immune cell infiltration analysis and GSEA between low- and high-risk groups

ESTIMATE, TIMER, ssGSEA, and MCP-counter methods were utilized to compare the degree of immune infiltration between the two risk groups in TCGA-LUAD. Firstly, ESTIMATE analysis revealed that the high-risk group had significantly lower ImmuneScore, StromalScore, and ESTIMATEScore than low-risk group (Fig. 6A), indicating lower immune cell infiltration in the TME of LUAD patients with a high risk. TIMER analysis demonstrated that in comparison to low-risk group, the score of Macrophage was lower in high-risk group (Fig. 6B), implying that the function of Macrophage was inhibited in high-risk patients. The infiltration of 28 types of immune cells was further explored through ssGSEA, and it was observed that compared to low-risk group, the infiltration of most immune cells (such as plasmacytoid dendritic cell,

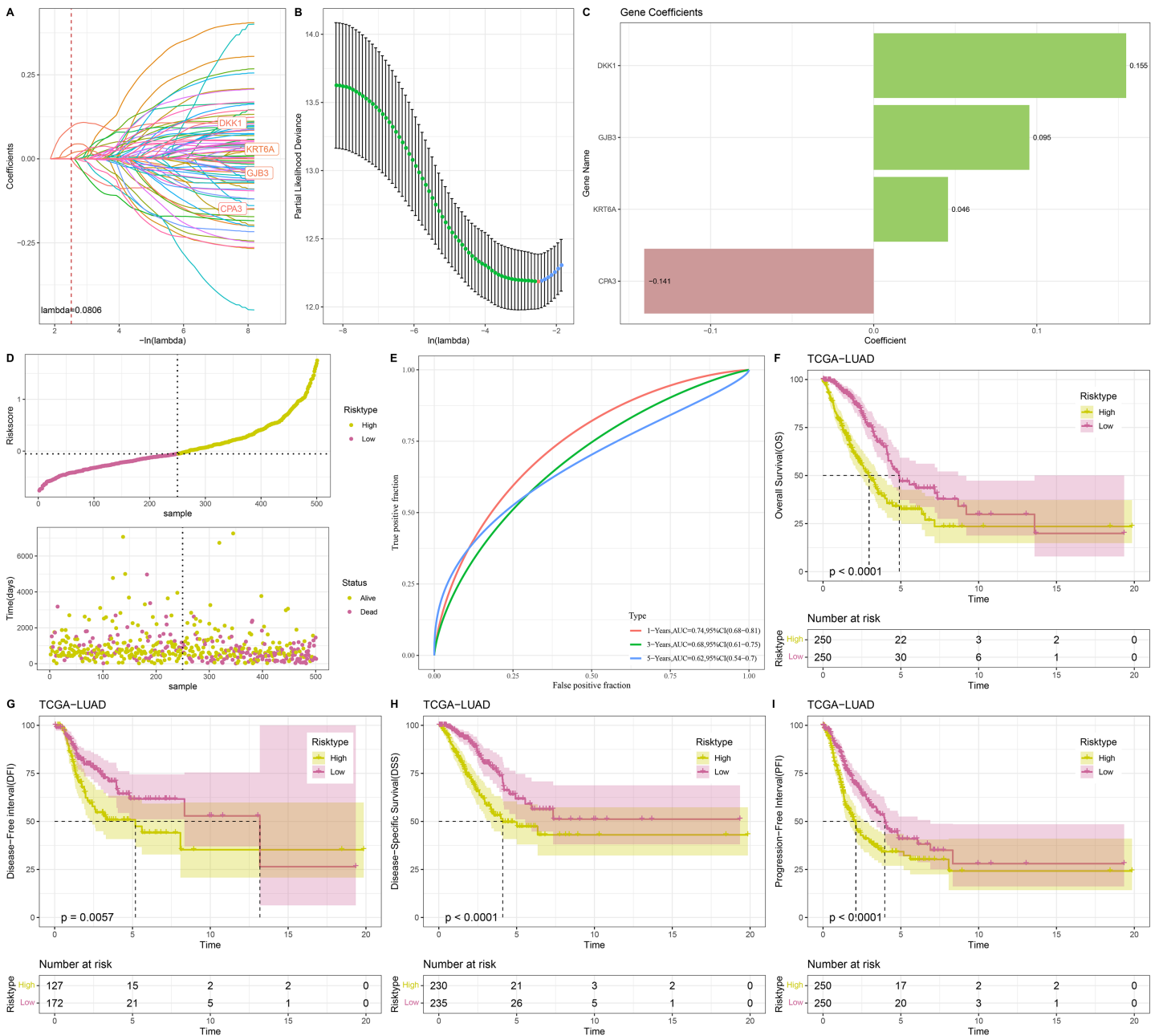


Figure 4 Construction and evaluation of RiskScore model. (A, B) Results of narrowing the gene range through LASSO. (C) The coefficients of four independent prognostic NMRGs in TCGA-LUAD cohort. (D) RiskScore of samples in TCGA-LUAD cohort. (E) ROC curve of RiskScore model for 1-, 3-, and 5-years in TCGA-LUAD cohort. (F-I) Kaplan-Meier curves of OS, disease-free interval (DFI), disease-specific survival (DSS), and progression-free interval (PFI) between two risk groups in TCGA-LUAD cohort. [Full-size DOI: 10.7717/peerj.18991/fig-4](https://doi.org/10.7717/peerj.18991/fig-4)

eosinophil, immature dendritic cell, activated CD4 T cell, mast cell, immature B cell, monocyte, natural killer cell, activated B cell) was remarkably lower in high-risk group (Fig. 6C), suggesting an immunosuppressive environment in the high-risk group. Furthermore, MCP-counter analysis demonstrated that the infiltration of neutrophil, T cell, endothelial cell, myeloid dendritic cell and B lineage were significantly reduced in

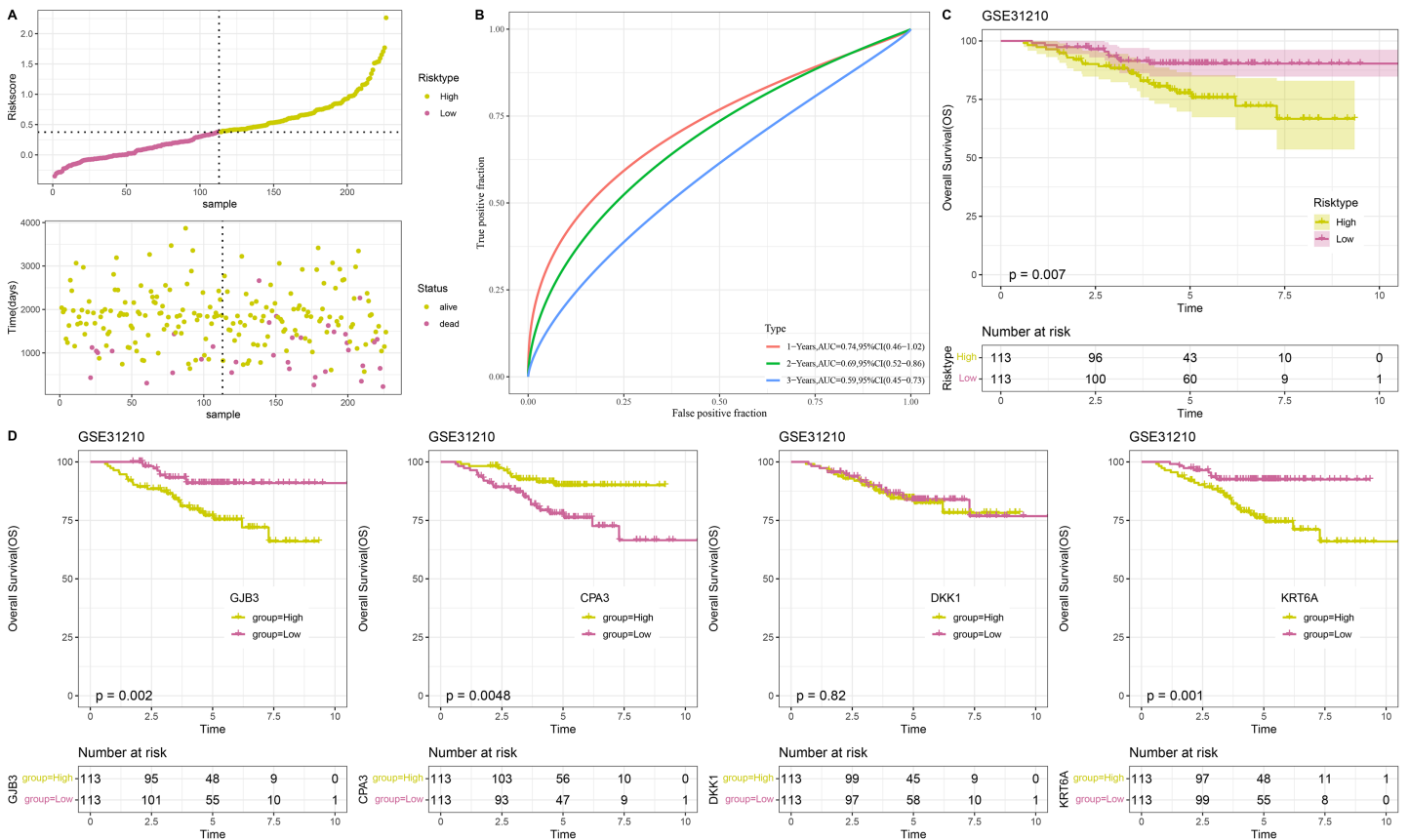


Figure 5 Validation of RiskScore model. (A) RiskScore of samples in GSE31210 dataset. (B) ROC curve of RiskScore model for 1-, 3-, and 5-years in GSE31210 dataset. (C) OS curve of two risk groups in GSE31210 dataset. (D) The relationship between high/low expression groups of four independent prognostic NMRGs and OS in GSE31210 dataset. Full-size [DOI: 10.7717/peerj.18991/fig-5](https://doi.org/10.7717/peerj.18991/fig-5)

high-risk group (Fig. 6D). The GSEA results showed that the low-risk group was primarily enriched in allograft rejection and bile acid metabolism, whereas the high-risk group was more enriched in numerous HALLMARK pathways (Fig. 7).

High-risk group exhibited poor immunotherapy response and drug sensitivity

With the purpose to further investigate the potential value of the NMRG signature in the precision treatment of LUAD, the efficacy of immunotherapy and 10 common chemotherapy drugs for different risk groups of TCGA-LUAD patients was analyzed. It was found that the TIDE score of high-risk patients was notably higher (Fig. 8A) and the ratio of responders to immunotherapy in this group was lower (Fig. 8B), showing that high-risk LUAD patients had greater immune escape capabilities and less active immunotherapy responses. Additionally, the IC_{50} values of Erlotinib, Paclitaxel, Cisplatin, Saracatinib, and CGP_082996 in high-risk group were lower than that in low-risk group (Fig. 8C), which indicated that these drugs were more effective in treating high-risk LUAD patients. However, high-risk LUAD patients exhibited low sensitivities to Rapamycin, PHA_665752, Sorafenib, Imatinib, and Crizotinib.

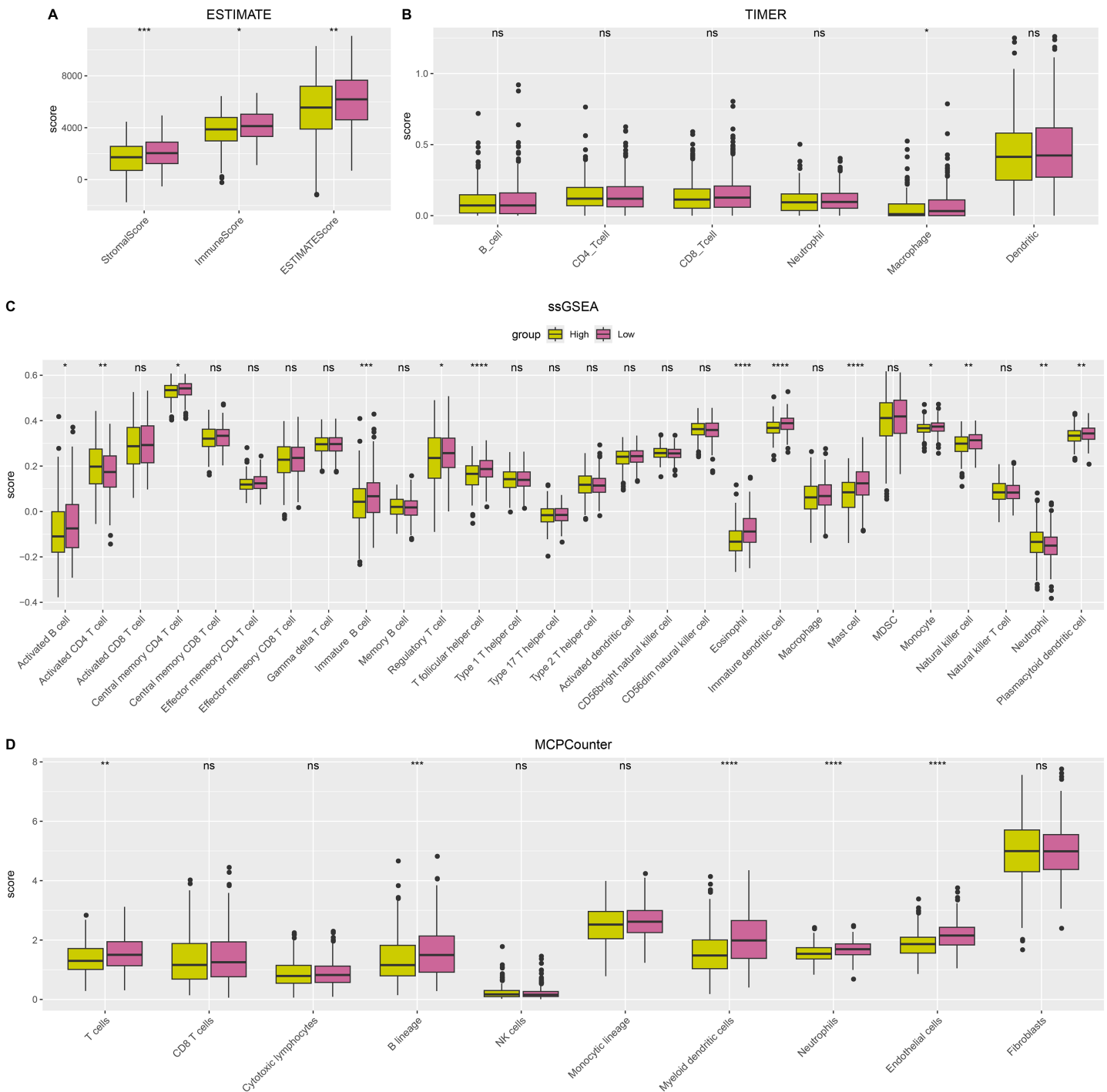


Figure 6 The difference of tumor microenvironment (TME) between two risk groups in TCGA-LUAD cohort. (A) StromalScore, ImmuneScore, and ESTIMATEScore evaluated by ESTIMATE method. (B) The scores of six immune cells assessed by TIMER method. (C) The scores of 28 immune cells calculated by ssGSEA. (D) The scores of 10 immune cells computed by MCP-counter analysis. **** means $p < 0.0001$; *** means $p < 0.001$; ** means $p < 0.01$; * means $p < 0.05$; ns means not significant. [Full-size !\[\]\(b345a1c4255362eec3746050dd71ccac_img.jpg\) DOI: 10.7717/peerj.18991/fig-6](https://doi.org/10.7717/peerj.18991/fig-6)

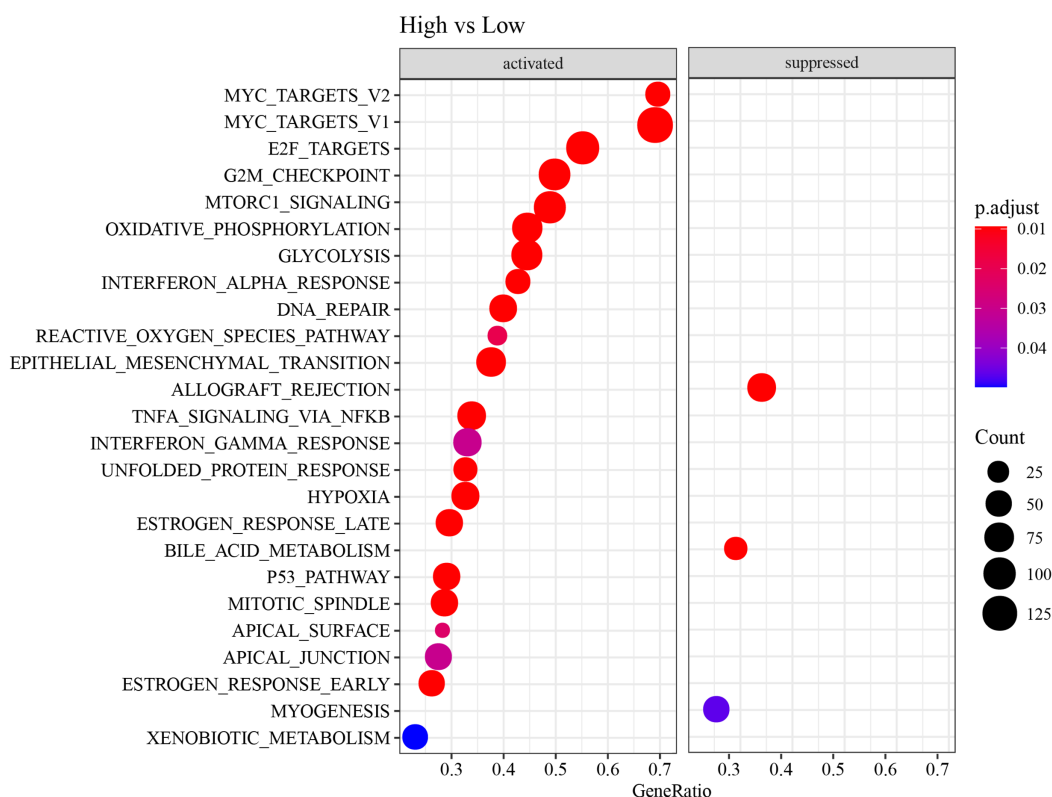


Figure 7 HALLMARK pathway enrichment results of DEGs between two risk groups.

Full-size [DOI: 10.7717/peerj.18991/fig-7](https://doi.org/10.7717/peerj.18991/fig-7)

A nomogram with an excellent prediction performance was established

The univariate and multivariate Cox regression analysis verified that N.stage, RiskScore, and T.stage were independent factors for LUAD prognosis (Figs. 9A and 9B). Then, a nomogram was established, and the RiskScore exhibited the strongest influence on the prediction of survival probability (Fig. 9C). In addition, calibration curve showed that 1-year, 3-year, and 5-year calibration points were close to the ideal curves (Fig. 9D). According to DCA, the benefits of the nomogram were significantly higher than the baseline model (Fig. 9E), emphasizing the potential value of the nomogram in clinical decision-making. Moreover, the C-index of the nomogram was also higher than that of clinical features and RiskScore (Fig. 9F), which further confirmed its accurate prediction ability. The ROC curve of the nomogram was plotted, with an AUC value of 0.924 (Fig. 9G), which reflected a strong diagnostic performance of the nomogram.

Silencing *GJB3* inhibited the migration and invasion of LUAD cells

The data from qRT-PCR revealed that the mRNA expressions of *GJB3*, *DKK1*, *CPA3*, and *KRT6A* were all notably upregulated in A549 cells than in BEAS-2B cells (Figs.10A–10D). *GJB3* is a member of a group of proteins known as connexins, which fulfill crucial functions in the formation of channels and connections and in turn support the

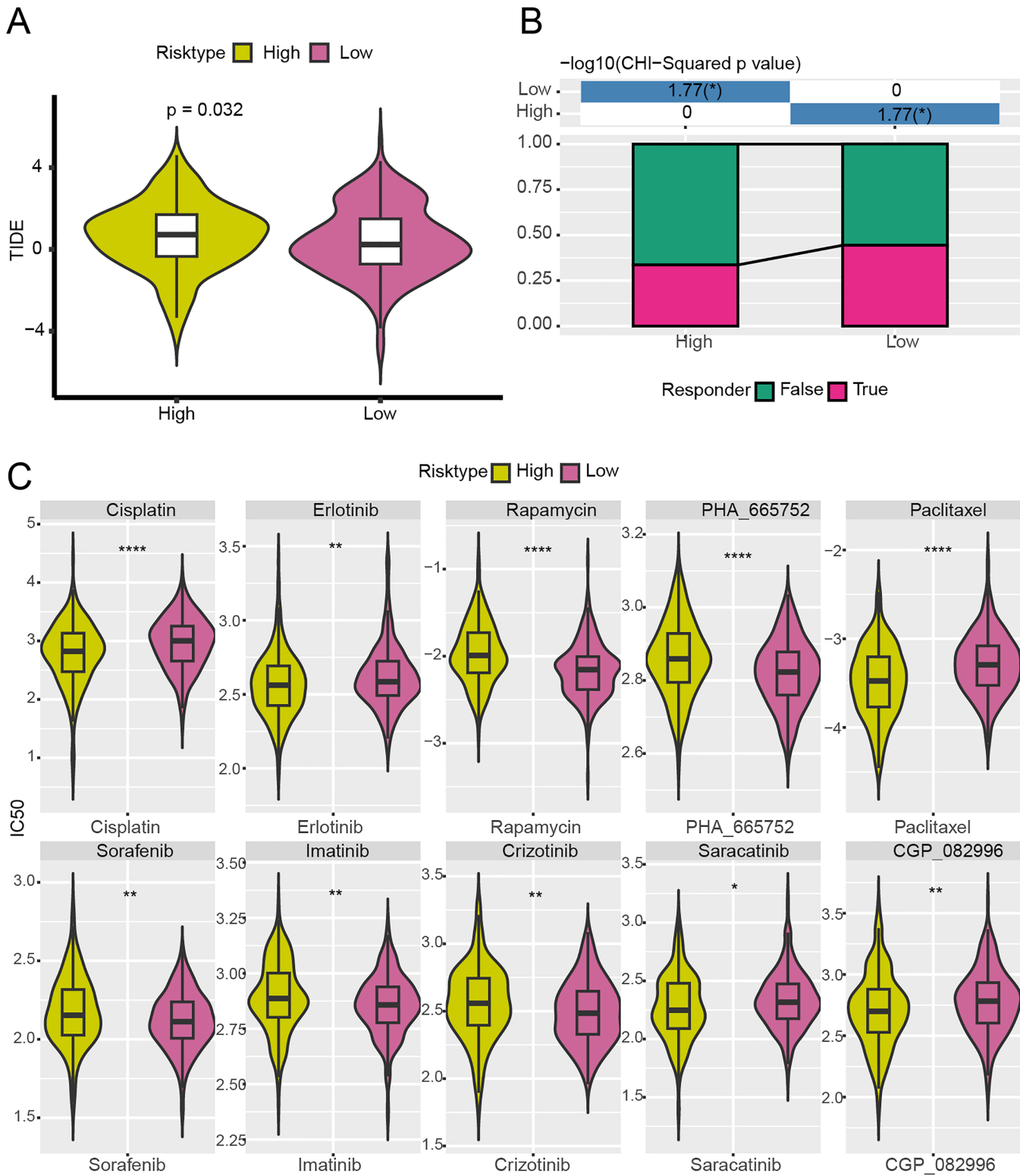


Figure 8 Analysis of immunotherapy response and drug sensitivity between two risk groups in TCGA-LUAD cohort. (A) The difference of TIDE score between two risk groups in TCGA-LUAD cohort. (B) The proportion of responders to immunotherapy between two risk groups in TCGA-LUAD cohort. (C) The difference of drug sensitivity between two risk groups in TCGA-LUAD cohort. **** means $p < 0.0001$; ** means $p < 0.01$; * means $p < 0.05$. [Full-size !\[\]\(fd7fe780e8fd8eece60268c87d0c3e04_img.jpg\) DOI: 10.7717/peerj.18991/fig-8](https://doi.org/10.7717/peerj.18991/fig-8)

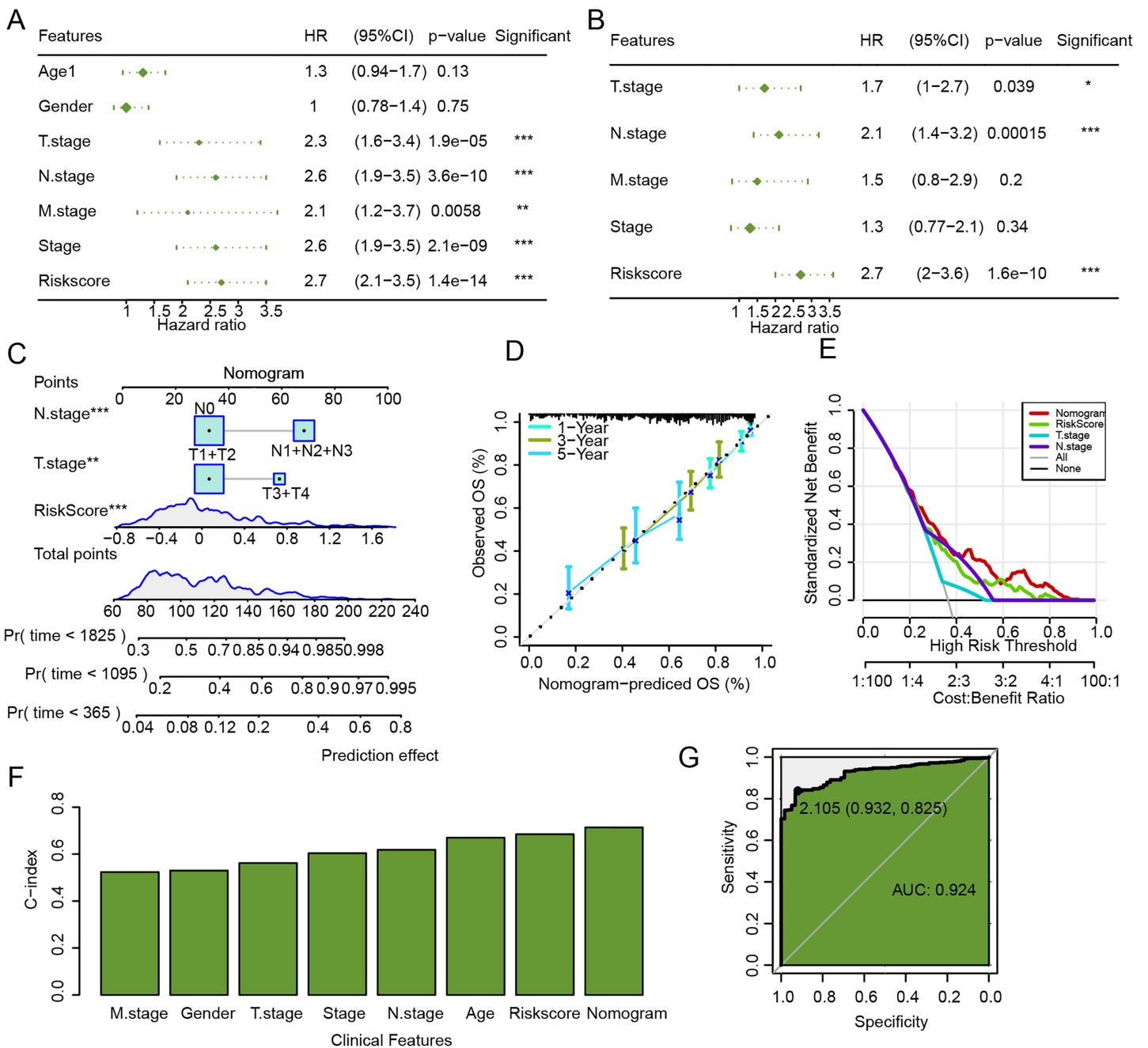


Figure 9 Establishment and assessment of nomogram combining RiskScore and clinical features. (A) Univariate Cox regression analysis of RiskScore and clinical features. (B) Multivariate Cox regression analysis of RiskScore and clinical features. (C) Nomogram established by combining RiskScore and clinical features. (D) Calibration curve of nomogram. (E) Decision curve of nomogram. (F) C-index of clinical features, RiskScore, and nomogram. (G) ROC curve of nomogram. Full-size [DOI: 10.7717/peerj.18991/fig-9](https://doi.org/10.7717/peerj.18991/fig-9)

communication between cells (Zeng *et al.*, 2024). However, the role of *GJB3* in cancers has been less studied, particularly LUAD. Here, the wound healing and Transwell assays demonstrated that the silencing of *GJB3* reduced the numbers of migrated and invaded A549 cells (Figs.10E and 10F).

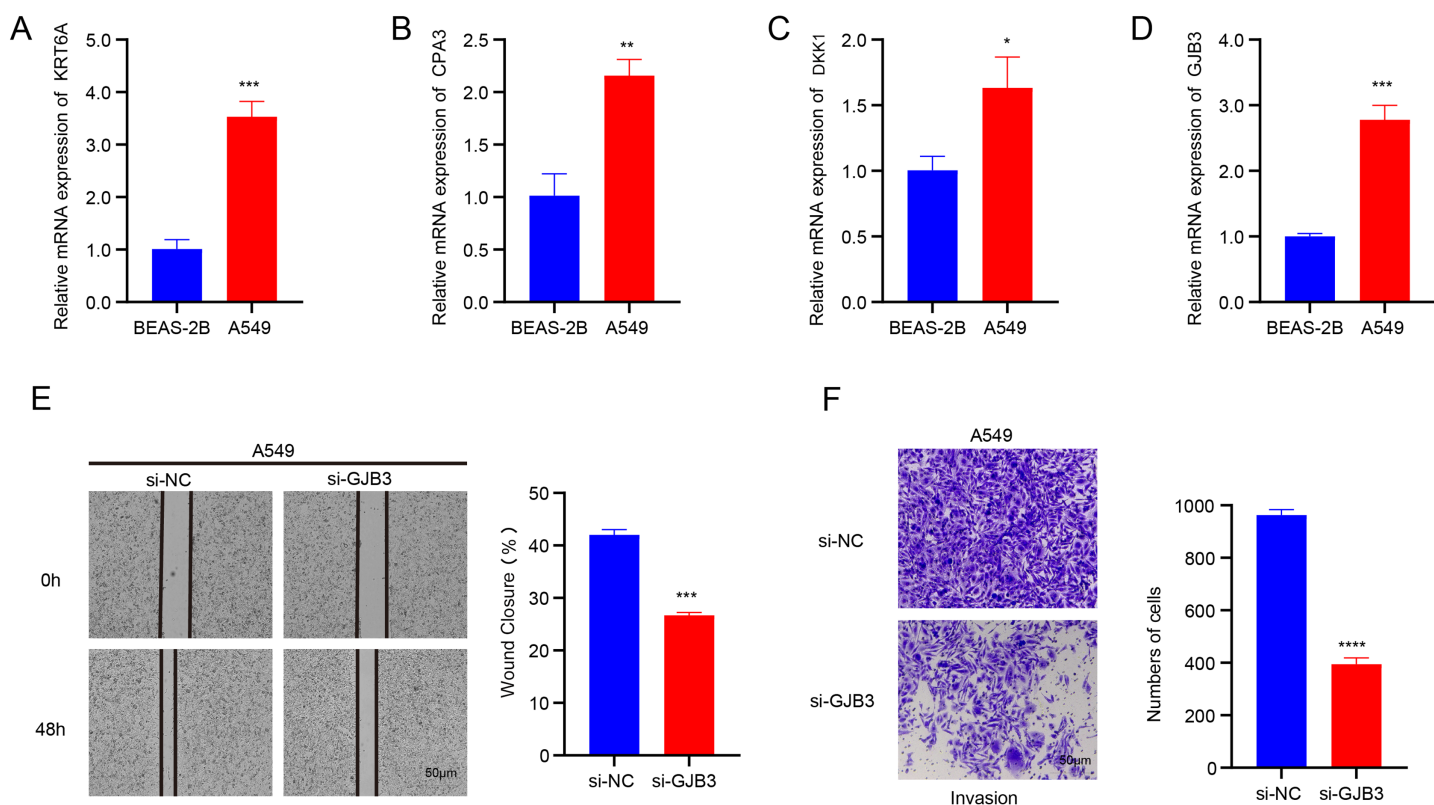


Figure 10 Validation assay *in vitro* using LUAD cells. (A-D) The mRNA expression levels of four independent prognostic NMRGs, *KRT6A*, *CPA3*, *DKK1*, and *GJB3*, in LUAD cells A549 and normal lung epithelial cells BEAS-2B by qRT-PCR. (E) The impact of *GJB3* silencing on the migration of LUAD cells A549 evaluated by wound healing assay. (F) The effect of *GJB3* silencing on the invasion of LUAD cells A549 detected by Transwell assay. **** means $p < 0.0001$; *** means $p < 0.001$; ** means $p < 0.01$; * means $p < 0.05$. [Full-size !\[\]\(fcc3264021d438d9732560e78099f674_img.jpg\) DOI: 10.7717/peerj.18991/fig-10](https://doi.org/10.7717/peerj.18991/fig-10)

DISCUSSION

Increased energy metabolism in cells has been linked to the initiation and progression of tumors by numerous studies (Park et al., 2012; Ullah et al., 2024). NAM is well-recognized as a crucial regulator of REDOX processes and mitochondrial function, thereby playing a key role in managing cellular energy metabolism. An accumulating body of evidence supports the involvement of NAM in cancer prevention and treatment (Chen et al., 2015). Recently, there has been a significant focus on the role of NAM in both the diagnosis and therapeutic strategies for tumors. For example, Yang et al. (2024) identified NAM-related genes applying bioinformatics analysis to predict the survival of patients with hepatocellular carcinoma. However, research on the role of NAM in LUAD remains limited. This study delineated LUAD subtypes with NAM-related genes. We performed differential gene analysis and functional characterization to determine key genes and to develop a risk model that can effectively predict the immunotherapy response and prognosis of LUAD patients. Subsequently, we also evaluated the prognosis, immune cell infiltration and immunotherapy response of patients with LUAD categorized into different risk groups by the RiskScore model.

This study delineated two subtypes (C1 and C2) of LUAD based on the NMRGs, with C2 subtype exhibiting a better prognosis than C1 subtype. In comparison to C2 subtype,

more patients in C1 subtype were in the pathologic_M1, pathologic_T3, T4, pathologic_N1, N2, and pathologic_stage II, III. *TTN* and *FLG* were the genes with higher mutation frequencies in both C1 and C2. Specifically, the frequency of *TTN* mutation was higher in C2 than in C1, while that of *FLG* was higher in C1 than that in C2. *TTN* is the largest protein that plays crucial roles in the structure, development, mechanics, and regulation of cardiac and skeletal muscles (Chauveau, Rowell & Ferreiro, 2014). *FLG* is a filaggrin protein critical for the formation of the stratum corneum (Yicheng et al., 2022). Studies have confirmed that mutations in *TTN* and *FLG* are closely involved in the occurrence of LUAD and its prognosis (Xue et al., 2021; Hasan et al., 2015; Cheng et al., 2019). Therefore, different mutation frequencies of the two genes may account for the prognostic differences between C1 and C2, but further in-depth research is required to validate the hypothesis. In addition, C1 subtype was associated with glycolytic metabolism-correlated pathways, while C2 subtype was more related to fatty acid metabolism pathway. These findings may offer a novel insight into the subtype classification and prognostic evaluation for LUAD patients based on NAM metabolism.

Furthermore, four independent prognostic NMRGs, including one protective gene (*CPA3*) and three risk genes (*DKK1*, *GJB3*, *KRT6A*), were screened to construct a RiskScore model. *CPA3* is a specific zinc metalloproteinase expressed in mast cells and is involved in the degradation of endogenous proteins (Hämäläinen et al., 2022; Feng, Fu & Nie, 2023). *DKK1*, a secretory Wnt antagonist, is upregulated in a variety of human malignancies (Zheng et al., 2022; Zhu et al., 2021). Previous research showed that high-expressed *DKK1* is indicative of a worse prognosis in LUAD (Li et al., 2023). *GJB3* belongs to the gap junction protein family and encodes junction protein 31 (Chen, Zhao & Hu, 2023). It has been found that high-expressed *GJB3* is closely linked to a worse prognosis in LUAD (Dou et al., 2024). This study also showed that *GJB3* was high-expressed in LUAD patients, and that the silencing of *GJB3* can inhibit the migration and invasion of LUAD cells. In addition, *GJB3* knockdown suppressed PI3K/AKT pathway activation and inhibited the proliferation, migration, and viability of a variety of cancer cells, including LUAD (Zeng et al., 2024). This suggested that the function of *GJB3* in the TME may be affected by the metabolic regulation of NAM, especially in regulating cell proliferation, apoptosis and immune cell infiltration. Huo et al. (2022) discovered that *GJB3* promotes liver metastasis of pancreatic cancer by enhancing neutrophil polarization and survival. Our study also found an upregulated expression of neutrophils in the high-risk group, indicating that *GJB3* facilitated tumor progression and metastasis through the modulation of neutrophil activity in high-risk LUAD patients. Zhou et al. (2021) demonstrated that the down-regulation of *KRT6A* expression mediated by siRNA inhibited the growth of non-small cell lung cancer (NSCLC) cells *in vivo*. Furthermore, high-expressed *KRT6A* may facilitate the proliferation and metastasis of LUAD *via* epithelial mesenchymal transformation (Sun et al., 2023). This indicated that NAM metabolism was involved in regulating cell proliferation and oxidative stress response, which may in turn affect the expression and function of *KRT6A* in cancer cells.

Additionally, *in vitro* experiments in this study revealed that the mRNA expressions of *DKK1*, *GJB3*, *KRT6A*, and *CPA3* in LUAD cell line A549 were significantly upregulated. Taken together, these findings further demonstrated that these four NMRGs were closely linked to LUAD and could be considered as biomarkers for LUAD.

Cancer cells undergo metabolic reprogramming and consume resources within the TME, which consequently creates a microenvironment hostile to the survival and functionality of immune cells (Yang *et al.*, 2020). This metabolic competition offers novel targets for immunotherapy. By targeting the metabolic processes of cancer cells, it is possible to indirectly improve the function and survival of immune cells, thereby potentially enhancing immunotherapy outcomes (Cerezo & Rocchi, 2020). In this study, immune infiltration analysis demonstrated that the expressions of most immune cell types in the high-risk group were lower than the low-risk group. This suggested that the high-risk group may promote tumor cell evasion from immune surveillance by inhibiting the infiltration and activity of immune cells within the TME. Furthermore, the high-risk group was enriched in numerous HALLMARK pathways, indicating broad abnormalities in biological processes. Patients categorized into the low-risk group typically exhibited lower TIDE scores and were more likely to respond to immunotherapy. Conversely, the high-risk group showed higher sensitivity to some chemotherapeutic agents such as Erlotinib, Paclitaxel, Cisplatin, Saracatinib, and CGP_082996. Notably, Cisplatin, which treats a variety of solid tumors including LUAD (Galanski, 2006), functions by triggering DNA damage responses and mitochondrial apoptosis (Galluzzi *et al.*, 2012). Erlotinib, used for NSCLC and pancreatic cancer, inhibits tumor cell division, leading to cell cycle arrest and programmed cell death in tumor cells (Abdelgalil, Al-Kahtani & Al-Jenoobi, 2020). Saracatinib is a Src kinase inhibitor. Src is a non-receptor tyrosine kinase closely related to growth factor and cytokine receptors and plays a pivotal role in invasion, motility, tumor cell adhesion, and angiogenesis (Thomas & Brugge, 1997). Studies have shown its effectiveness in the treatment of SCLC (Molina *et al.*, 2014). These findings suggested that the low-risk group was more likely to benefit from immunotherapy, while high-risk group was more suitable for taking chemotherapeutic drugs, providing valuable insights for personalized treatment of patients with LUAD.

Despite the insight gained from our research, several limitations must be acknowledged. Firstly, the sample size of the TCGA-LUAD and GSE31210 datasets used in this study was relatively small, and future research should prioritize validating our findings in larger cohorts. Moreover, there is a need for cellular and animal model experiments to analyze the changes in NAM metabolism under different knockdown conditions, alongside assessments of the expressions of immune-related molecules on cell surface and the killing activity of immune cells. Experiments as such will help determine the pathways through which the genes affect the immune regulation in LUAD. Furthermore, the establishment of an *in vitro* co-culture model of LUAD cells and immune cells such as T cells at a specific ratio could stimulate the TME more accurately. This setup would allow for the observation of cell interaction and further clarify the association between NAM metabolism and immune escape.

CONCLUSION

This study identified four prognostic biomarkers closely associated with LUAD and examined the correlation between the expressions of these biomarkers and the clinical features of LUAD patients. Our results highlighted variations in treatment sensitivity across different risk groups. These findings deepen our understanding of the pathogenesis and progression of LUAD and provide crucial guidance for the improvement of personalized treatment of the cancer. By adopting stratified treatment based on risk groups, we can more accurately select suitable therapeutic interventions, which could improve the treatment efficacy and the survival of LUAD patients. The current findings significantly contribute to the precision and personalization of LUAD treatment.

ABBREVIATIONS

OS	overall survival
C-index	consistency index
NMRGs	NAM metabolism-related genes
ROS	reactive oxygen species
qRT-PCR	quantitative real-time polymerase chain reaction
DCA	decision curve analysis
ICIs	immune checkpoint inhibitors
TIICs	tumor infiltration immune cells
GSEA	gene set enrichment analysis
NAD⁺	nicotinamide-adenine dinucleotide
FC	FoldChange
ROC	receiver operating characteristic
TME	tumor microenvironment
FPKM	Fragments Per Kilobase per Million
TIMER	tumor immune estimation resource
si	small interfering
AUC	area under ROC curve
IC₅₀	half maximal inhibitory concentration
TIDE	tumor immune dysfunction and exclusion
Gln	glutamine
CDF	cumulative distribution function
DSS	disease-specific survival
ssGSEA	single sample gene set enrichment analysis
MsigDB	Molecular Signature Database
LUAD	lung adenocarcinoma
FBS	fetal bovine serum
DEGs	differentially expressed genes
AAMRGS	amino acid metabolism-related gene signature
NAM	Nicotinamide
GEO	Gene Expression Omnibus

MCP-counter	microenvironment cell populations-counter
WHO	World Health Organization
DFI	disease-free interval
PD-L1	programmed cell death ligand 1
PD-1	programmed cell death protein-1
ESTIMATE	Estimation of STromal and Immune cells in MAlignant Tumours using Expression data
TCGA	The Cancer Genome Atlas
NAMPT	NAM phosphoribosyltransferase
PFI	progression-free interval
NSCLC	non-small cell lung cancer

ADDITIONAL INFORMATION AND DECLARATIONS

Funding

The study was supported by Tianjin Health Science and Technology Project (No. TJWJ2024XK016) and Tianjin Key Medical Discipline (Specialty) Construction Project (No. TIYXZDXK-018A). The funders had no role in study design, data collection and analysis, decision to publish, or preparation of the manuscript.

Grant Disclosures

The following grant information was disclosed by the authors:

Tianjin Health Science and Technology: TJWJ2024XK016.

Tianjin Key Medical Discipline (Specialty) Construction: TIYXZDXK-018A.

Competing Interests

The authors declare that they have no competing interests.

Author Contributions

- Meng Wang performed the experiments, analyzed the data, authored or reviewed drafts of the article, and approved the final draft.
- Wei Li conceived and designed the experiments, authored or reviewed drafts of the article, and approved the final draft.
- Fang Zhou conceived and designed the experiments, analyzed the data, prepared figures and/or tables, and approved the final draft.
- Zheng Wang performed the experiments, prepared figures and/or tables, authored or reviewed drafts of the article, and approved the final draft.
- Xiaoteng Jia performed the experiments, prepared figures and/or tables, and approved the final draft.
- Xingpeng Han analyzed the data, authored or reviewed drafts of the article, and approved the final draft.

Data Availability

The following information was supplied regarding data availability:

The datasets generated and/or analyzed during the current study are available at NCBI: [GSE31210](https://www.ncbi.nlm.nih.gov/geo/query/acc.cgi?acc=GSE31210).

The experimental data is available in GitHub and Zenodo:

- <https://github.com/1XingpengHan/Raw-data-for-submitting.git>.

- 1XingpengHan. (2024). 1XingpengHan/Raw-data-for-submitting: Raw data (v.1.1.0). Zenodo. <https://doi.org/10.5281/zenodo.14032899>.

Supplemental Information

Supplemental information for this article can be found online at <http://dx.doi.org/10.7717/peerj.18991#supplemental-information>.

REFERENCES

- Abdelgalil AA, Al-Kahtani HM, Al-Jenoobi FI. 2020.** Chapter four-Erlotinib. In: Brittain HG, ed. *Profiles of Drug Substances, Excipients and Related Methodology*. Vol. 45, 93–117.
- Burgos ES. 2011.** NAMPT in regulated NAD biosynthesis and its pivotal role in human metabolism. *Current Medicinal Chemistry* **18**(13):1947–1961
DOI [10.2174/092986711795590101](https://doi.org/10.2174/092986711795590101).
- Cao K, Ling X, Jiang X, Ma J, Zhu J. 2022.** Pan-cancer analysis of UBE2T with a focus on prognostic and immunological roles in lung adenocarcinoma. *Respiratory Research* **23**:306
DOI [10.1186/s12931-022-02226-z](https://doi.org/10.1186/s12931-022-02226-z).
- Cao X, Wu B, Hou Y, Chen J. 2023.** Lipid metabolism-related gene signatures for predicting the prognosis of lung adenocarcinoma. *Translational Cancer Research* **12**(8):2099–2114
DOI [10.21037/tcr-23-375](https://doi.org/10.21037/tcr-23-375).
- Cao H, Xue Y, Wang F, Li G, Zhen Y, Guo J. 2024.** Identification of prognostic molecular subtypes and model based on CD8+ T cells for lung adenocarcinoma. *Biocell* **48**(3):473–490
DOI [10.32604/biocell.2024.048946](https://doi.org/10.32604/biocell.2024.048946).
- Cerezo M, Rocchi S. 2020.** Cancer cell metabolic reprogramming: a keystone for the response to immunotherapy. *Cell Death & Disease* **11**(11):1734 DOI [10.1038/s41419-020-03175-5](https://doi.org/10.1038/s41419-020-03175-5).
- Chauveau C, Rowell J, Ferreiro A. 2014.** A rising titan: review and mutation update. *Human Mutation* **35**(9):1046–1059 DOI [10.1002/humu.22611](https://doi.org/10.1002/humu.22611).
- Chen AC, Martin AJ, Choy B, Fernández-Peñas P, Dalziel RA, McKenzie CA, Scolyer RA, Dhillon HM, Vardy JL, Krickler A, St George G, Chinniah N, Halliday GM, Damian DL. 2015.** A phase 3 randomized trial of nicotinamide for skin-cancer chemoprevention. *The New England Journal of Medicine* **373**(17):1618–1626 DOI [10.1056/NEJMoa1506197](https://doi.org/10.1056/NEJMoa1506197).
- Chen Q, Zhao H, Hu J. 2023.** A robust six-gene prognostic signature based on two prognostic subtypes constructed by chromatin regulators is correlated with immunological features and therapeutic response in lung adenocarcinoma. *Aging* **15**(21):12330–12368
DOI [10.18632/aging.205183](https://doi.org/10.18632/aging.205183).
- Cheng X, Yin H, Fu J, Chen C, An J, Guan J, Duan R, Li H, Shen H. 2019.** Aggregate analysis based on TCGA: TTN missense mutation correlates with favorable prognosis in lung squamous cell carcinoma. *Journal of Cancer Research and Clinical Oncology* **145**(4):1027–1035
DOI [10.1007/s00432-019-02861-y](https://doi.org/10.1007/s00432-019-02861-y).
- Cui H, Ren X, Dai L, Chang L, Liu D, Zhai Z, Kang H, Ma X. 2023.** Comprehensive analysis of nicotinamide metabolism-related signature for predicting prognosis and immunotherapy

- response in breast cancer. *Frontiers in Immunology* **14**:1145552
DOI [10.3389/fimmu.2023.1145552](https://doi.org/10.3389/fimmu.2023.1145552).
- Ding Y, Lv J, Hua Y. 2022.** Comprehensive metabolomic analysis of lung cancer patients treated with Fu Zheng Fang. *Current Pharmaceutical Analysis* **18(9)**:881–891
DOI [10.2174/1573412918666220822143119](https://doi.org/10.2174/1573412918666220822143119).
- Dou R, Liu R, Su P, Yu X, Xu Y. 2024.** The GJB3 correlates with the prognosis, immune cell infiltration, and therapeutic responses in lung adenocarcinoma. *Open Medicine* **19(1)**:20240974
DOI [10.1515/med-2024-0974](https://doi.org/10.1515/med-2024-0974).
- Fan M, Lu L, Shang H, Lu Y, Yang Y, Wang X, Lu H. 2024.** Establishment and verification of a prognostic model based on coagulation and fibrinolysis-related genes in hepatocellular carcinoma. *Aging* **16(9)**:7578–7595 DOI [10.18632/aging.205699](https://doi.org/10.18632/aging.205699).
- Faubert B, Solmonson A, DeBerardinis RJ. 2020.** Metabolic reprogramming and cancer progression. *Science* **368(6487)**:eaaw5473 DOI [10.1126/science.aaw5473](https://doi.org/10.1126/science.aaw5473).
- Feng J, Fu F, Nie Y. 2023.** Comprehensive genomics analysis of aging related gene signature to predict the prognosis and drug resistance of colon adenocarcinoma. *Frontiers in Pharmacology* **14**:1121634 DOI [10.3389/fphar.2023.1121634](https://doi.org/10.3389/fphar.2023.1121634).
- Feng Y, Tang L, Wang H, Liu Y, Yang S, Lin L, Hu X, Shi Y. 2023.** Immune checkpoint inhibitors combined with angiogenic inhibitors in the treatment of locally advanced or metastatic lung adenocarcinoma patients. *Cancer Immunology, Immunotherapy: CII* **72**:449–459
DOI [10.1007/s00262-022-03251-z](https://doi.org/10.1007/s00262-022-03251-z).
- Galanski MS. 2006.** Recent developments in the field of anticancer platinum complexes. *Recent Patents on Anti-Cancer Drug Discovery* **1(2)**:285–295 DOI [10.2174/157489206777442287](https://doi.org/10.2174/157489206777442287).
- Galluzzi L, Senovilla L, Vitale I, Michels J, Martins I, Kepp O, Castedo M, Kroemer G. 2012.** Molecular mechanisms of cisplatin resistance. *Oncogene* **31(15)**:1869–1883
DOI [10.1038/onc.2011.384](https://doi.org/10.1038/onc.2011.384).
- Guo X, Zhang Y, Liu C, Ren L, Gao S, Bi J, Liang J, Wang P. 2022.** Intranasal administration of β -1, 3-galactosyltransferase 2 confers neuroprotection against ischemic stroke by likely inhibiting oxidative stress and NLRP3 inflammasome activation. *The FASEB Journal* **36(10)**:e22542 DOI [10.1096/fj.202200456RR](https://doi.org/10.1096/fj.202200456RR).
- Hasan AN, Ahmad MW, Madar IH, Grace BL, Hasan TN. 2015.** An in silico analytical study of lung cancer and smokers datasets from gene expression omnibus (GEO) for prediction of differentially expressed genes. *Bioinformatics* **11(5)**:229–235 DOI [10.6026/97320630011229](https://doi.org/10.6026/97320630011229).
- He S, Tian J, Zang J, Long L, Liu P, Zhang Y, Xiao J. 2024.** Implications of intestinal microecology and immune function alterations for immunotherapy outcomes in advanced unresectable lung adenocarcinoma. *The Clinical Respiratory Journal* **18(5)**:e13762
DOI [10.1111/crj.13762](https://doi.org/10.1111/crj.13762).
- Hu F, Peng J, Niu Y, Mao X, Zhao Y, Jiang L. 2022.** Clinical predictors of treatment efficacy and a prognostic nomogram in patients with lung adenocarcinoma receiving immune checkpoint inhibitors: a retrospective study. *Journal of Thoracic Disease* **14(10)**:4096–4112
DOI [10.21037/jtd-22-1270](https://doi.org/10.21037/jtd-22-1270).
- Huo Y, Zhou Y, Zheng J, Jin G, Tao L, Yao H, Zhang J, Sun Y, Liu Y, Hu L-P. 2022.** GJB3 promotes pancreatic cancer liver metastasis by enhancing the polarization and survival of neutrophil. *Frontiers in Immunology* **13**:875 DOI [10.3389/fimmu.2022.983116](https://doi.org/10.3389/fimmu.2022.983116).
- Hämäläinen S, Kareinen L, Sukura A, Kareinen I. 2022.** Carboxypeptidase A3 expression in canine mast cell tumors and tissue-resident mast cells. *Veterinary Pathology* **59(2)**:236–243
DOI [10.1177/03009858211062636](https://doi.org/10.1177/03009858211062636).

- Innis SE, Reinaltt K, Civelek M, Anderson WD. 2021. GSEApilot: a package for customizing gene set enrichment analysis in R. *Journal of Computational Biology: A Journal of Computational Molecular Cell Biology* 28(6):629–631 DOI 10.1089/cmb.2020.0426.
- Jia S, Zhai L, Wu F, Lv W, Min X, Zhang S, Li F. 2024. Integrative machine learning algorithms for developing a consensus RNA modification-based signature for guiding clinical decision-making in bladder cancer. *Oncologie* 26(2):269–285 DOI 10.1515/oncologie-2023-0348.
- Jung M, Lee KM, Im Y, Seok SH, Chung H, Kim DY, Han D, Lee CH, Hwang EH, Park SY, Koh J, Kim B, Nikas IP, Lee H, Hwang D, Ryu HS. 2022. Nicotinamide (niacin) supplement increases lipid metabolism and ROS-induced energy disruption in triple-negative breast cancer: potential for drug repositioning as an anti-tumor agent. *Molecular Oncology* 16(9):1795–1815 DOI 10.1002/1878-0261.13209.
- Ke ZB, Wu YP, Huang P, Hou J, Chen YH, Dong RN, Lin F, Wei Y, Xue XY, Ng CF, Xu N. 2021. Identification of novel genes in testicular cancer microenvironment based on ESTIMATE algorithm-derived immune scores. *Journal of Cellular Physiology* 236:706–713 DOI 10.1002/jcp.29898.
- Li Q, Chu Y, Yao Y, Song Q. 2024. A Treg-related riskscore model may improve the prognosis evaluation of colorectal cancer. *The Journal of Gene Medicine* 26(2):e3668 DOI 10.1002/jgm.3668.
- Li HD, Deng C, Zhang XQ, Lin CX. 2023. A gene set-integrated approach for predicting disease-associated genes. *IEEE/ACM Transactions on Computational Biology and Bioinformatics* 20(6):3440–3450 DOI 10.1109/TCBB.2022.3214517.
- Li M, Kirtane AR, Kiyokawa J, Nagashima H, Lopes A, Tirmizi ZA, Lee CK, Traverso G, Cahill DP, Wakimoto H. 2020. Local targeting of NAD(+) salvage pathway alters the immune tumor microenvironment and enhances checkpoint immunotherapy in glioblastoma. *Cancer Research* 80(22):5024–5034 DOI 10.1158/0008-5472.CAN-20-1094.
- Li X, Liu M, Liu H, Chen J. 2022. Tumor metabolic reprogramming in lung cancer progression. *Oncology Letters* 24(2):287 DOI 10.3892/ol.2022.13407.
- Li Q, Wang T, Zhu J, Zhang A, Wu A, Zhou Y, Shi J. 2023. A cuproptosis-related lncRNAs risk model to predict prognosis and guide immunotherapy for lung adenocarcinoma. *Annals of Translational Medicine* 11(5):198 DOI 10.21037/atm-22-3195.
- Li J, Xie L, Xie Y, Wang F. 2020. Bregmannian consensus clustering for cancer subtypes analysis. *Computer Methods and Programs in Biomedicine* 189:105337 DOI 10.1016/j.cmpb.2020.105337.
- Lin Z, He Y, Wu Z, Yuan Y, Li X, Luo W. 2023. Comprehensive analysis of copper-metabolism-related genes about prognosis and immune microenvironment in osteosarcoma. *Scientific Reports* 13:15059 DOI 10.1038/s41598-023-42053-w.
- Liu Z, Wang R, Wang Y, Duan Y, Zhan H. 2023. Targeting succinylation-mediated metabolic reprogramming as a potential approach for cancer therapy. *Biomedicine & Pharmacotherapy* 168(1):115713 DOI 10.1016/j.biopha.2023.115713.
- Liu Z, Zhang M, Cao X, Ma M, Han B. 2024. Anoikis-related gene signatures predict prognosis of lung adenocarcinoma patients and reveal immune infiltration. *Translational Cancer Research* 13(4):1861–1875 DOI 10.21037/tcr-23-2185.
- Lv H, Lv G, Chen C, Zong Q, Jiang G, Ye D, Cui X, He Y, Xiang W, Han Q, Tang L, Yang W, Wang H. 2021. NAD(+) metabolism maintains inducible PD-L1 expression to drive tumor immune evasion. *Cell Metabolism* 33(1):110–127.e5 DOI 10.1016/j.cmet.2020.10.021.

- Meng X, Zhao X, Zhou B, Song W, Liang Y, Liang M, Du M, Shi J, Gao Y. 2024.** FSTL3 is associated with prognosis and immune cell infiltration in lung adenocarcinoma. *Journal of Cancer Research and Clinical Oncology* **150(1)**:17 DOI [10.1007/s00432-023-05553-w](https://doi.org/10.1007/s00432-023-05553-w).
- Molina JR, Foster NR, Reungwetwattana T, Nelson GD, Grainger AV, Steen PD, Stella PJ, Marks R, Wright J, Adjei AA. 2014.** A phase II trial of the Src-kinase inhibitor saracatinib after four cycles of chemotherapy for patients with extensive stage small cell lung cancer: NCCTG trial N-0621. *Lung Cancer* **85(2)**:245–250 DOI [10.1016/j.lungcan.2014.03.004](https://doi.org/10.1016/j.lungcan.2014.03.004).
- Nguyen TT, Lee HS, Burt BM, Wu J, Zhang J, Amos CI, Cheng C. 2022.** A lepidic gene signature predicts patient prognosis and sensitivity to immunotherapy in lung adenocarcinoma. *Genome Medicine* **14**:5 DOI [10.1186/s13073-021-01010-w](https://doi.org/10.1186/s13073-021-01010-w).
- Nikas IP, Paschou SA, Ryu HS. 2020.** The role of nicotinamide in cancer chemoprevention and therapy. *Biomolecules* **10(3)**:477 DOI [10.3390/biom10030477](https://doi.org/10.3390/biom10030477).
- Nong S, Han X, Xiang Y, Qian Y, Wei Y, Zhang T, Tian K, Shen K, Yang J, Ma X. 2023.** Metabolic reprogramming in cancer: mechanisms and therapeutics. *MedComm* **4(2)**:e218 DOI [10.1002/mco2.218](https://doi.org/10.1002/mco2.218).
- Park SY, Lee KB, Lee MJ, Bae SC, Jang JJ. 2012.** Nicotinamide inhibits the early stage of carcinogen-induced hepatocarcinogenesis in mice and suppresses human hepatocellular carcinoma cell growth. *Journal of Cellular Physiology* **227(3)**:899–908 DOI [10.1002/jcp.22799](https://doi.org/10.1002/jcp.22799).
- Saba NF, Dinasarapu AR, Magliocca KR, Dwivedi B, Seby S, Qin ZS, Patel M, Griffith CC, Wang X, El-Deiry M, Steuer CE, Kowalski J, Shin DM, Zwick ME, Chen ZG. 2020.** Signatures of somatic mutations and gene expression from p16INK4A positive head and neck squamous cell carcinomas (HNSCC). *PLOS ONE* **15(9)**:e0238497 DOI [10.1371/journal.pone.0238497](https://doi.org/10.1371/journal.pone.0238497).
- Shahrajabian MH, Sun W. 2023.** Survey on multi-omics, and multi-omics data analysis, integration and application. *Current Pharmaceutical Analysis* **19(4)**:267–281 DOI [10.2174/1573412919666230406100948](https://doi.org/10.2174/1573412919666230406100948).
- Shum HCE, Wu K, Vadgama J, Wu Y. 2023.** Potential therapies targeting the metabolic reprogramming of diabetes-associated breast cancer. *Journal of Personalized Medicine* **13(1)**:157 DOI [10.3390/jpm13010157](https://doi.org/10.3390/jpm13010157).
- Song HJ, Kim T, Choi HN, Kim SJ, Lee SD. 2023.** TonEBP expression is essential in the IL-1 β -induced migration and invasion of human A549 lung cancer cells. *Oncology Research* **32(1)**:151–161 DOI [10.32604/or.2023.030690](https://doi.org/10.32604/or.2023.030690).
- Song SB, Park JS, Chung GJ, Lee IH, Hwang ES. 2019.** Diverse therapeutic efficacies and more diverse mechanisms of nicotinamide. *Metabolomics: Official Journal of the Metabolomic Society* **15(10)**:137 DOI [10.1007/s11306-019-1604-4](https://doi.org/10.1007/s11306-019-1604-4).
- Song Z, Yu J, Wang M, Shen W, Wang C, Lu T, Shan G, Dong G, Wang Y, Zhao J. 2023.** CHDTEPDB: transcriptome expression profile database and interactive analysis platform for congenital heart disease. *Congenital Heart Disease* **18(6)**:693–701 DOI [10.32604/chd.2024.048081](https://doi.org/10.32604/chd.2024.048081).
- Sun K, Zhang Z, Wang D, Huang Y, Zhang J, Lian C. 2023.** Regulation of early diagnosis and prognostic markers of lung adenocarcinoma in immunity and hypoxia. *Scientific Reports* **13(1)**:6459 DOI [10.1038/s41598-023-33404-8](https://doi.org/10.1038/s41598-023-33404-8).
- Tang Z, Wang L, Wu G, Qin L, Tan Y. 2023.** FGD5 as a novel prognostic biomarker and its association with immune infiltrates in lung adenocarcinoma. *Biocell* **47(11)**:2503–2516 DOI [10.32604/biocell.2023.031565](https://doi.org/10.32604/biocell.2023.031565).
- Thomas SM, Brugge JS. 1997.** Cellular functions regulated by Src family kinases. *Annual Review of Cell and Developmental Biology* **13(1997)**:513–609 DOI [10.1146/annurev.cellbio.13.1.513](https://doi.org/10.1146/annurev.cellbio.13.1.513).

- Travelli C, Consonni FM, Sangaletti S, Storto M, Morlacchi S, Grolla AA, Galli U, Tron GC, Portararo P, Rimassa L, Pressiani T, Mazzone M, Trovato R, Ugel S, Bronte V, Tripodo C, Colombo MP, Genazzani AA, Sica A. 2019. Nicotinamide phosphoribosyltransferase acts as a metabolic gate for mobilization of myeloid-derived suppressor cells. *Cancer Research* 79(8):1938–1951 DOI 10.1158/0008-5472.CAN-18-1544.
- Ullah A, Razzaq A, Alfaifi MY, Elbehairi SEI, Mena F, Ullah N, Shehzadi S, Nawaz T, Iqbal H. 2024. Sanguinarine attenuates lung cancer progression via oxidative stress-induced cell apoptosis. *Current Molecular Pharmacology* 17:e18761429269383 DOI 10.2174/0118761429269383231119062233.
- Wang C, Wu X, Chen H, Le Q, Dai L. 2022. A nomogram for predicting overall survival in patients with follicular thyroid cancer after thyroidectomy: a SEER database analysis. *Gland Surgery* 11(8):1356–1366 DOI 10.21037/gs-22-386.
- Wang H, You S, Fang M, Fang Q. 2020. Recognition of immune microenvironment landscape and immune-related prognostic genes in breast cancer. *BioMed Research International* 2020:3909416 DOI 10.1155/2020/3909416.
- Wu J, Li L, Zhang H, Zhao Y, Zhang H, Wu S, Xu B. 2021. A risk model developed based on tumor microenvironment predicts overall survival and associates with tumor immunity of patients with lung adenocarcinoma. *Oncogene* 40(26):4413–4424 DOI 10.1038/s41388-021-01853-y.
- Xia X, Ge Y, Ge F, Gu P, Liu Y, Li P, Xu P. 2024. MAP4 acts as an oncogene and prognostic marker and affects radioresistance by mediating epithelial-mesenchymal transition in lung adenocarcinoma. *Journal of Cancer Research and Clinical Oncology* 150(2):88 DOI 10.1007/s00432-024-05614-8.
- Xu H, Chen HC, Yang L, Yang G, Liang L, Yang Y, Tang H, Bao H, Wu X, Shao Y, An G, Wang Y. 2023. Mutational landscape of SWI/SNF complex genes reveal correlation to predictive biomarkers for immunotherapy sensitivity in lung adenocarcinoma patients. *ESMO Open* 8(3):101585 DOI 10.1016/j.esmoop.2023.101585.
- Xue D, Lin H, Lin L, Wei Q, Yang S, Chen X. 2021. TTN/TP53 mutation might act as the predictor for chemotherapy response in lung adenocarcinoma and lung squamous carcinoma patients. *Translational Cancer Research* 10(3):1284–1294 DOI 10.21037/tcr-20-2568.
- Yang S, Li A, Lv L, Duan J, Zheng Z, Zhuo W, Min J, Wei J. 2024. Identification and validation of nicotinamide metabolism-related gene signatures as a novel prognostic model for hepatocellular carcinoma. *OncoTargets and Therapy* 17:423–438 DOI 10.2147/OTT.S464709.
- Yang R, Li X, Wu Y, Zhang G, Liu X, Li Y, Bao Y, Yang W, Cui H. 2020. EGFR activates GDH1 transcription to promote glutamine metabolism through MEK/ERK/ELK1 pathway in glioblastoma. *Oncogene* 39(14):2975–2986 DOI 10.1038/s41388-020-1199-2.
- Yi M, Li A, Zhou L, Chu Q, Luo S, Wu K. 2021. Immune signature-based risk stratification and prediction of immune checkpoint inhibitor's efficacy for lung adenocarcinoma. *Cancer Immunology, Immunotherapy* 70(6):1705–1719 DOI 10.1007/s00262-020-02817-z.
- Yicheng F, Xin L, Tian Y, Huilin L. 2022. Association of FLG mutation with tumor mutation load and clinical outcomes in patients with gastric cancer. *Frontiers in Genetics* 13:17036 DOI 10.3389/fgene.2022.808542.
- Zeng J, Li X, Zhang Y, Zhang B, Wang H, Bao S, Zu L, Zhang H, Cheng Y, Tang Q, Xu X, Xu S, Song Z. 2024. GJB3: a comprehensive biomarker in pan-cancer prognosis and immunotherapy prediction. *Aging* 16(9):7647–7667 DOI 10.18632/aging.205774.

- Zhang ZF. 2022.** A novel pyroptosis scoring model was associated with the prognosis and immune microenvironment of esophageal squamous cell carcinoma. *Frontiers in Genetics* **13**:1034606 DOI [10.3389/fgene.2022.1034606](https://doi.org/10.3389/fgene.2022.1034606).
- Zhang H, Shan G, Jin X, Yu X, Bi G, Feng M, Wang H, Lin M, Zhan C, Wang Q, Li M. 2022.** ARNTL2 is an indicator of poor prognosis, promotes epithelial-to-mesenchymal transition and inhibits ferroptosis in lung adenocarcinoma. *Translational Oncology* **26**:101562 DOI [10.1016/j.tranon.2022.101562](https://doi.org/10.1016/j.tranon.2022.101562).
- Zhang C, Wang L, Ren G, Xu G, Li R, Xie H, Cui Z. 2023.** Modulation of Bleomycin-induced oxidative stress and pulmonary fibrosis by ginkgetin in mice via AMPK. *Current Molecular Pharmacology* **16**(2):217–227 DOI [10.2174/1874467215666220304094058](https://doi.org/10.2174/1874467215666220304094058).
- Zhang L, Yi H, Chen J, Li H, Luo Y, Cheng T, Yang H, Jiang Z, Pan C. 2022.** Neutrophil extracellular traps facilitate A549 cell invasion and migration in a macrophage-maintained inflammatory microenvironment. *BioMed Research International* **2022**:8316525 DOI [10.1155/2022/8316525](https://doi.org/10.1155/2022/8316525).
- Zhang YJ, Zhao LY, He X, Yao RF, Lu F, Lu BN, Pang ZR. 2022.** CBXs-related prognostic gene signature correlates with immune microenvironment in gastric cancer. *Aging* **14**(15):6227–6254 DOI [10.18632/aging.204214](https://doi.org/10.18632/aging.204214).
- Zhang J, Zou S, Fang L. 2023.** Metabolic reprogramming in colorectal cancer: regulatory networks and therapy. *Cell & Bioscience* **13**:25 DOI [10.1186/s13578-023-00977-w](https://doi.org/10.1186/s13578-023-00977-w).
- Zheng K, Hai Y, Chen H, Zhang Y, Hu X, Ni K. 2024.** Tumor immune dysfunction and exclusion subtypes in bladder cancer and pan-cancer: a novel molecular subtyping strategy and immunotherapeutic prediction model. *Journal of Translational Medicine* **22**:365 DOI [10.1186/s12967-024-05186-8](https://doi.org/10.1186/s12967-024-05186-8).
- Zheng Y, Su Y, Ruan L, He Q, Gong L, Li J. 2023.** Screening and biomarker assessment of ferroptosis genes FLT3 and ALOX5 in lung adenocarcinoma. *Oncologie* **25**(3):281–289 DOI [10.1515/oncologie-2023-0090](https://doi.org/10.1515/oncologie-2023-0090).
- Zheng Y, Zhou Z, Wei R, Xiao C, Zhang H, Fan T, Zheng B, Li C, He J. 2022.** The RNA-binding protein PCBP1 represses lung adenocarcinoma progression by stabilizing DKK1 mRNA and subsequently downregulating β -catenin. *Journal of Translational Medicine* **20**:343 DOI [10.1186/s12967-022-03552-y](https://doi.org/10.1186/s12967-022-03552-y).
- Zhou J, Jiang G, Xu E, Zhou J, Liu L, Yang Q. 2021.** Identification of SRXN1 and KRT6A as key genes in smoking-related non-small-cell lung cancer through bioinformatics and functional analyses. *Frontiers in Oncology* **11**:810301 DOI [10.3389/fonc.2021.810301](https://doi.org/10.3389/fonc.2021.810301).
- Zhou B, Zhu W, Yuan S, Wang Y, Zhang Q, Zheng H, Zhu L, Xu J. 2022.** High GNG4 expression is associated with poor prognosis in patients with lung adenocarcinoma. *Thoracic Cancer* **13**(3):369–379 DOI [10.1111/1759-7714.14265](https://doi.org/10.1111/1759-7714.14265).
- Zhu G, Song J, Chen W, Yuan D, Wang W, Chen X, Liu H, Su H, Zhu J. 2021.** Expression and role of Dickkopf-1 (Dkk1) in tumors: from the cells to the patients. *Cancer Management and Research* **13**:659–675 DOI [10.2147/CMAR.S275172](https://doi.org/10.2147/CMAR.S275172).